NRL Report 8051

A Fidelity and Stability Investigation of Solid-State Transceiver Modules

HARRY E. BARLOW

Airborne Radar Branch
Radar Division

November 1, 1976

NAVAL RESEARCH LABORATORY
Washington, D.C.

SECURITY CLASSIFICATION OF THIS PAGE *(When Data Entered)*

REPORT DOCUMENTATION PAGE

READ INSTRUCTIONS BEFORE COMPLETING FORM

1. REPORT NUMBER: NRL Report 8051	2. GOVT ACCESSION NO.
3. RECIPIENT'S CATALOG NUMBER	
4. TITLE *(and Subtitle)*: A FIDELITY AND STABILITY INVESTIGATION OF SOLID-STATE TRANSCEIVER MODULES	5. TYPE OF REPORT & PERIOD COVERED: A Final report on one phase of a continuing NRL problem
	6. PERFORMING ORG. REPORT NUMBER
7. AUTHOR(s): Harry E. Barlow	8. CONTRACT OR GRANT NUMBER(s)
9. PERFORMING ORGANIZATION NAME AND ADDRESS: Naval Research Laboratory, Washington, DC 20375	10. PROGRAM ELEMENT, PROJECT, TASK AREA & WORK UNIT NUMBERS: NRL Problem R02-29, Project WF 12-141-601, 62712N
11. CONTROLLING OFFICE NAME AND ADDRESS: Naval Air Systems Command, Washington, DC 20360	12. REPORT DATE: November 1, 1976
	13. NUMBER OF PAGES: 39
14. MONITORING AGENCY NAME & ADDRESS*(if different from Controlling Office)*	15. SECURITY CLASS. *(of this report)*: Unclassified
	15a. DECLASSIFICATION/DOWNGRADING SCHEDULE

16. DISTRIBUTION STATEMENT *(of this Report)*

Approved for public release; distribution unlimited.

17. DISTRIBUTION STATEMENT *(of the abstract entered in Block 20, if different from Report)*

18. SUPPLEMENTARY NOTES

19. KEY WORDS *(Continue on reverse side if necessary and identify by block number)*

Solid state modules
Microwave transceivers
Time sidelobes
Fidelity
Stability
AEW Radar
Spectral analysis

20. ABSTRACT *(Continue on reverse side if necessary and identify by block number)*

The pulse-to-pulse replication fidelity of solid-state microwave transceiver modules was investigated in terms of performance parameters of an AEW system. The overall distortion introduced by representative state-of-the-art modules was categorized and measured. A first-order time-domain analysis was made, relating nonideal module phase and amplitude response variations which occur as a function of the operating bandwidth to the system time-sidelobe response.

(Continued)

DD FORM 1 JAN 73 1473 EDITION OF 1 NOV 65 IS OBSOLETE
S/N 0102-014-6601

SECURITY CLASSIFICATION OF THIS PAGE *(When Data Entered)*

20. Abstract (Continued)

Pulse trains consisting of various numbers of contiguous pulses were recorded, and spectral analyses were performed on the recorded data. The measurement apparatus used a carrier-suppression technique to permit observation of the relatively low levels of module-induced distortion. It was found that the level of distortion introduced by the module was significantly below (some 13 to 16 dB lower than) values which might affect the detection capability of present-day AEW systems.

CONTENTS

A FIDELITY AND STABILITY INVESTIGATION OF SOLID-STATE TRANSCEIVER MODULES

INTRODUCTION

The purpose of this investigation was to determine, in terms of system performance, the pulse replication fidelity of groups of existing solid-state transceiver modules to determine their suitability for a future airborne early warning (AEW) coherent-MTI radar with pulse compression. The function of the module, both in the transmit and receive modes, is to amplify a linear frequency-modulated rectangular pulse (chirp). In the process of amplification, a typical module will introduce some noise and distortion. This tends to degrade the level of performance of the entire AEW system. This experimental investigation sought to quantify the degradation introduced by representative state-of-the-art modules.

The overall distortion introduced by the module can be separated conveniently into the following categories:

- Pulse-amplitude droop,
- Pulse-phase droop,
- Ripple content in the amplitude of the waveform,
- Ripple content in the phase of the waveform,
- The results of deviations from a linear phase characteristic over the frequency band, and
- Spurious oscillations (including instabilities related to the rise and fall-times).

The first four distortions have been treated by numerous authors [1-3]. A first-order time-domain analysis of the fifth mechanism is included in this report. The last mechanism, which has received little attention to date, is brought into play by the frequency modulation and rise/fall times of the signals typically used for AEW application. The theoretical analysis of this mechanism is extremely complex, because of nonlinearity, and has not been addressed in this work. The effort reported here has been concentrated on observation of the aggregate distortion arising from all sources and determination of the power level of that distortion relative to the level of the carrier.

A doppler radar distinguishes moving-target returns from fixed-target returns by the frequency characteristics of the return signals. A return from a target having a radial velocity relative to the radar will experience a frequency shift f_d which is proportional to that velocity. The two-way doppler frequency shift is given by $f_d = 2v/\lambda$, where λ is the wavelength of the signal transmitted by the radar and v is the radial velocity between the radar platform and the target.

Typically AEW radar operation requires the detection of targets over a wide range of velocities. It follows that the radar must respond to a correspondingly wide range of doppler frequencies. Doppler filters are used to separate the velocity range into smaller *velocity bins*. A signal at the output of the filter would indicate the radar has detected a target having a radial velocity relative to the radar platform that falls within the velocity bin or response of the filter. If the distortion introduced by the module results in a spurious signal occurring within the doppler frequency range, the system will be unable to distinguish it from a target and will generate a false target indication. MTI radar distinguishes a true target from clutter through comparison of target indications derived from successive pulses.

As will be seen later, the relative power level of the distortion introduced by the module will place an upper limit on the clutter rejection achievable. The figure-of-merit used to describe the performance of a given signal-processing technique is the improvement factor I, defined by $I = r_o/r_i$, where r_o is the power ratio of the target-to-clutter returns at the output of the processor, averaged over all target velocities, and r_i is the corresponding quantity at the input.

The basic limit on the improvement factor of the system is set by the variation of the radar signal from pulse to pulse. This variation can arise in a number of ways:

- Variation in the clutter characteristics with time,
- Variation in the propagation characteristics,
- Variation in the signal waveform presented to the transmit portion of the module,
- Variations arising in the transmit/receive sections of the module.

This last variation is of concern here.

In operation the radiated pulse illuminates a target. Some energy is reflected back in the direction of the radar and ultimately becomes an input to the processor. A train of these received pulses is processed as a group. This processing, for radar systems on a moving platform, will include compensation for platform motion. The processing scheme envisaged employs a precanceler followed by a coherent integrator. Ideally the residue from this processor is entirely attributable to target characteristics. If pulse-to-pulse variations are introduced by the module, a residue results which has the appearance of a target signal. Depending on the characteristics of this residue, the processor may treat it as a target-induced signal, which results in it being passed to the display, so that a false target results. In this way, amplitude and phase variations in the module characteristics place a limit on the detection capability of the radar.

Since the main emphasis here is the AEW application, the stability of prime interest is of short term. Short-term stability here refers to the stability of the system over the period of integration. Typically this is from 16 to 24 pulses, so that for a low-PRF radar the period over which stability is of interest is on the order of 0.1 second.

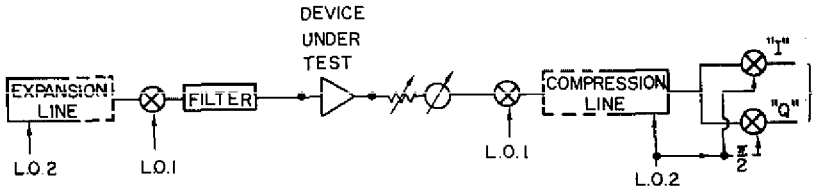

Fig. 1 — First version of the initial test setup developed at NRL

EXPERIMENTAL APPARATUS AND PROCEDURE

The experimental effort was in two phases. The first phase was performed at NRL and consisted initially of the construction of two versions of the test setup. Module-induced distortion was observed. The experimental technique was refined and verified to determine the best arrangement. The second phase, performed at RCA, Moorestown, N.J. [4], was a fully automated version of the earlier NRL experiment. The automated version of the experiment was designed to permit digital recording of the pulse-to-pulse data on a real-time basis. A PDP 11-40 computer was used for control of the RF circuitry, for timing, and for buffering the recorded data. The buffered data were then transferred to magnetic tapes, which were shipped to NRL for analysis.

Phase-One Experiment

The first of the two versions of the test setup employed at NRL is shown in Fig. 1. This version was an exploratory setup simply incorporating only the key components of an AEW system. It was primarily designed for a first look at the signals involved and to determine the order of magnitude of the distortion effects.

One of these key components was the pulse-expansion/compression filter network. This network uses surface-wave-device technology. It had previously been purchased by NRL from Hughes Aircraft Corporation for a space application and was made available by Mr. Brooks Dodson of the Space Sciences Division of NRL. This network operates at a center frequency of 40 MHz, and it provides an expanded pulse which is 120 μs wide with a bandwidth of 13 MHz and is linearly frequency modulated. The compression ratio of the network is 1000:1. When the expanded pulse is routed through the compression line, the compressed output pulse is 120 ns wide. The time sidelobes are approximately 22 dB down. The input power to compression network was kept at constant level for all tests. Figure 2 shows the expanded and compressed pulses.

The initial test setup was used to perform various tests on representative modules. These tests revealed that the distortion introduced by a typical module was quite small relative to the magnitude of the compressed pulse. This made measurement difficult, because the carrier tended to mask the much smaller distortion. Better resolution was needed to quantify the effects produced by the distortion. But this first configuration did allow a nearly instantaneous qualitative evaluation of modules. A malfunctioning module could be identified quickly and with little effort.

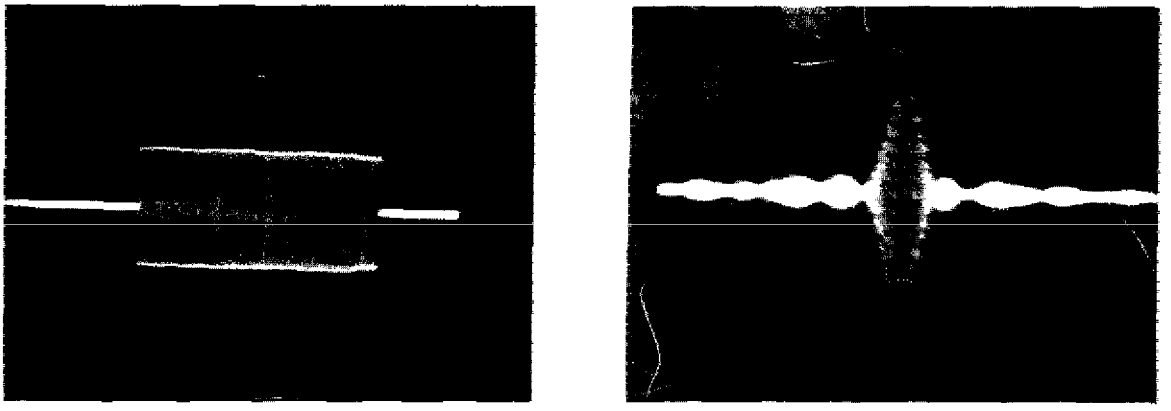

(a) Expanded (b) Compressed

Fig. 2 — Pulse outputs of the expansion/compression network

This initial test setup would be useful for production testing of modules, since it provides a quick and thorough analysis of a module's condition. Such a test would in most instances obviate the need for expensive and time-consuming point-by-point phase and amplitude response measurements. The time-domain response is indicative of the overall response of the module, and any substantial deviation from the normal response results in increased time-sidelobe levels or reduced peak main-lobe level. However for accurate determination of the distortion either greater dynamic-range or a lower signal-to-distortion ratio was required.

The desired signal-to-distortion ratio was achieved by suppressing the main signal pulse, this suppression being accomplished by modifying the original test setup through the incorporation of a nulling scheme. The modified version of the test setup, which will be referred to as the NRL time-sidelobe configuration, is shown in Fig. 3.

This modified version was employed by NRL for distortion testing of state-of-the-art modules made available by Mr. B. Dodson of the Space Sciences Division at NRL. A block diagram of one of these modules and photographs of its components are shown in Fig. 4. The device under test is placed in one arm of the bridge (Fig. 3), and a reference length of cable is placed in the other arm. Both arms also contain line-stretchers and attenuators for fine adjustment of the bridge.

An initial adjustment is made using all line stretchers and attenuators. In subsequent operation the reference arm is adjusted to obtain a maximum-depth null at the output of the bridge. When the maximum null is achieved, the residue at the output of the bridge theoretically consists of the distortion introduced by the module. Some leakage due to imperfect cancellation will generally be present.

For instance, when the module is excited with a CW type pulse (as opposed to the FM pulse normally used in the actual measurements) the reference arm of the bridge can be adjusted to achieve very low levels of power (60 dB less than the module output power) at the bridge output. When the same module is excited with a 13-MHz linear FM

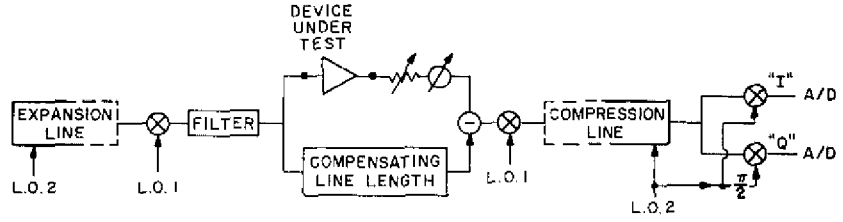

Fig. 3 — Second version (time-sidelobe configuration) of the initial test setup developed at NRL

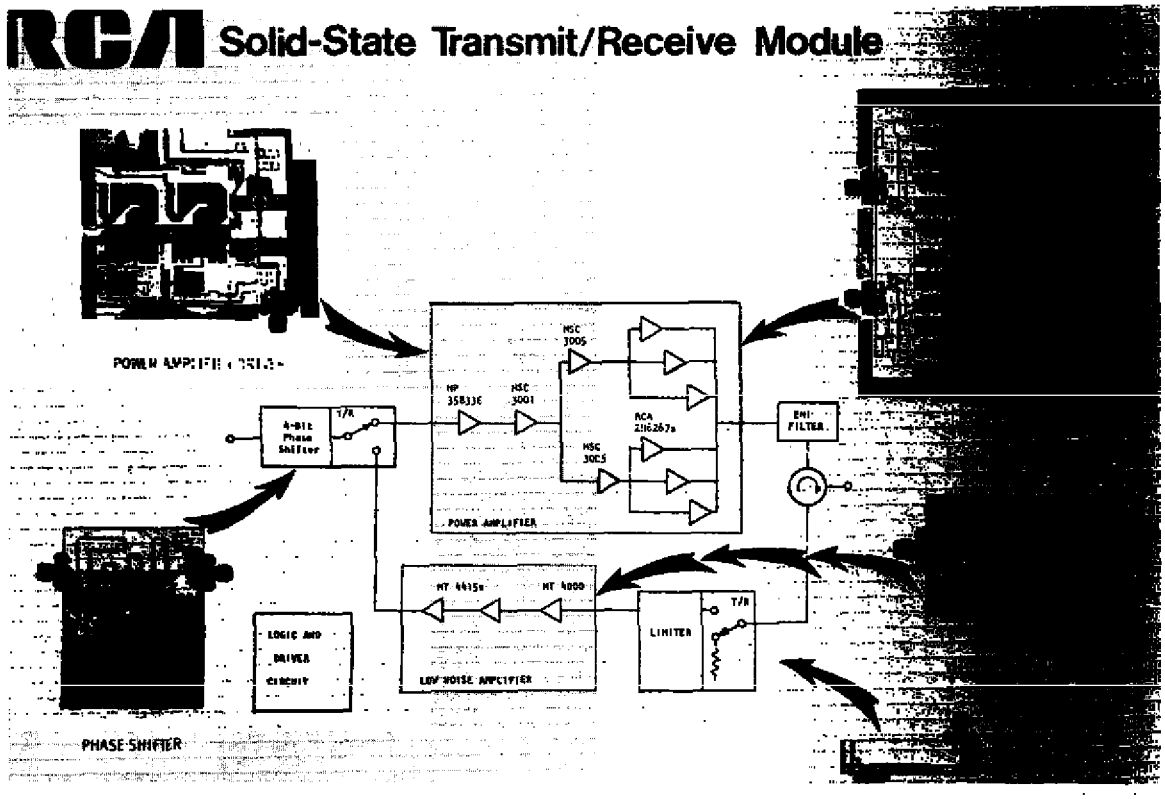

Fig. 4 — Solid-state transmit/receive (transceiver) module that was tested in phase one of this investigation

pulse, the depth of the null will be found to have degraded some 20 dB. This phenomenon is the result of two factors: one factor is that the module's response differs slightly from that of the reference arm, a property which is accentuated by the FM signal, and the other factor is that the module's response to the FM signal includes some spectral components not present in the reference arm of the bridge. While bridge was being adjusted to obtain a deep null, the bridge output or residue was observed on a spectrum analyzer and with a power meter. The nature of the nulls was such that the minimum-power condition could be achieved for two close-together but distinct reference-arm lengths (the depths of these nulls being identical to within 0.1 dB). The spectrum-analyzer presentation was used to ascertain which of the two settings of the reference arm which would result in the most uniform spectrum cancelation. This null-adjusting procedure was followed throughout both phases of the experiment.

When the bridge is adjusted for the deepest null, it is said to be in the balanced condition. In a given test the unbalanced conditions are identical to balanced conditions except that the reference arm has been opened and terminated in a 50-ohm load. Photographs showing the output of the compression network for the bridge in the balanced and unbalanced conditions are given in Fig. 5. These photographs were taken with RCA module 4 inserted in the bridge.

The Microwave Module Test Facility at NRL (Fig. 6a) was used to obtain phase and amplitude data on RCA module 4 (Fig. 6b). The test facility is a complex and sophisticated unit consisting of a number of custom and commercially available test equipments including the Hewlett-Packard Microwave Network Analyzer, Type 85420B and its associated computer. The facility is capable of automatically performing a large variety of tests on microwave modules while simultaneously performing a certain amount of analysis on the obtained data. The testing capability includes both CW and pulse-type measurements. The CW capability is primarily oriented toward receiver evaluation, and the pulse capability is oriented toward evaluation of higher power class-C transmitters. The obtained data can be simultaneously analyzed to generate such parameters as the mean, the average, the spread, and the system error.

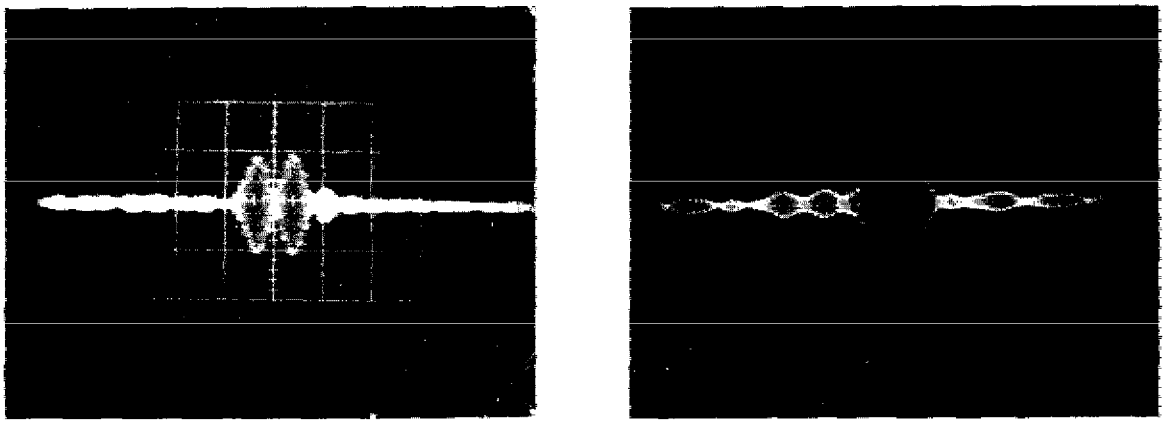

(a) Bridge in the balanced condition

(b) Bridge in the unbalanced condition

Fig. 5 — Compression-network output for the bridge of Fig. 3 with RCA module 4 inserted in the bridge as the device under test

Phase-Two Experiment

The second phase of the experimental effort was directed at obtaining pulse-to-pulse data on the distortion introduced by a module. The modules tested in this phase of the program were originally developed for the AFAR (Camel) Fractional Array Program (Contract F30602-C-0118). Emphasis was placed on the measurement of intrapulse variations in phase and amplitude and of pulse-to-pulse jitter. The results of these measurements at RCA were recorded on magnetic tapes, which were then sent to NRL for reduction and for eventual use in radar simulation programs under the [illegible] NRL.

The requirement for pulse-to-pulse data necessitated a substantial increase in the complexity of the test setup. This increased complexity resulted primarily from the incorporation of equipment to record in real time a sufficient number of individual consecutive pulses to provide useful resolution. To be useful, the recorded pulse trains had to be long in terms of the radar processing cycle. A maximum length of 128 consecutive pulses was chosen after due consideration of system factors and of the test equipment required.

Figure 7 is a block diagram of the configuration employed for all module measurements during phase two of the experiment. This test configuration will be referred to as the distortion test set (DTS). The DTS, in addition to the basic bridge circuit and the expansion/compression network, consisted of digital recording equipment, timing circuitry, electronically controlled switches, and a PDP 11-40 computer with its associated support equipment.

The digital recording equipment consists of synchronous detectors, analog-to-digital (A/D) converters, random access memories, interface circuitry, and some minor components such as couplers, filters, and video amplifiers. The synchronous detectors made up an in-phase and quadrature (I and Q) base-band mixer network. This network was used to detect the downconverted 40-MHz RF waveforms after they had been compressed.

The A/D converters were Computer Lab HS-810's, which are eight-bit bipolar devices. The A/D converters digitized the filtered and amplified I and Q outputs of the base-band mixer network, and each of these digitized outputs was then being routed to a random access memory (RAM), which served as interim storage. During the interval between pulses, the input/output (I/O) control unit transferred the set of data from the RAM to the core of the computer from which it is subsequently transferred to the magnetic tape. This procedure was necessary because of the limitations imposed by the magnetic-tape unit on the data rate. Low-pass filters were used to clean up the signals and perform the I and Q operations on them prior to the A/D operation. Video amplifiers and attenuators were used to obtain the proper signal level so as to maximize the dynamic range available from the A/D converters.

The timing circuitry included a master timer driven by a very stable and accurate 50-MHz synthesizer. The master timer is used in conjunction with a phase-lock loop and an impulse-gate generator to provide the necessary signals for synchronizing the various waveforms of the pulse expansion/compression network and the analog-to-digital sampling network.

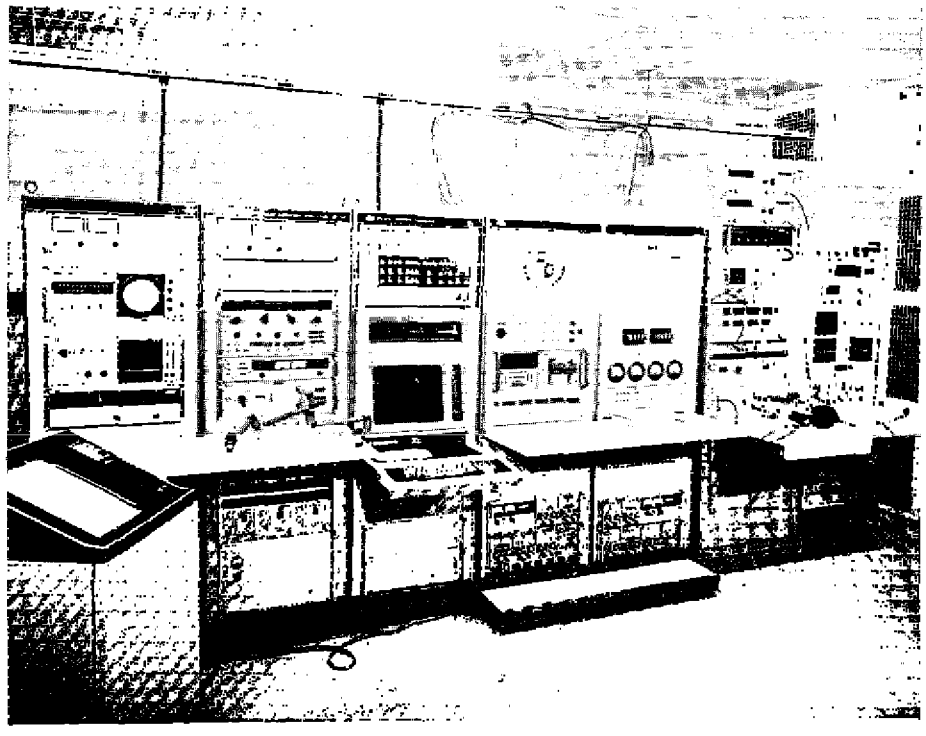

Fig. 6a — NRL Microwave Module Test Facility

This timing circuitry was necessitated in part by problems that occurred within the pulse-expansion/compression network after this phase of the experiment had begun. The envelope and the 40-MHz carrier which made up the expanded pulse were not in synchronism, and this resulted in a system jitter. This problem was thought to be brought about by the use of one-shot multivibrators in the timing circuits of the pulse expansion/compression network. Recognition of the inherently unstable character of multivibrators led to the installation of new circuits to drive the pulse-expansion/compression network. The new circuits derived their timing from the 50-MHz synthesizer, which provided excellent stability characteristics.

The DTS included electronically controlled RF switches and was designed so that it could be computer controlled. That is, the computer could automatically and quickly switch the DTS from one test mode to another. Computer control was advantageous because rapid switching greatly reduced any drift problems and because vast numbers of data could be taken in a short time.

In brief the DTS operates as follows when it is monitoring the compressed pulse. The master timer generates the signals to drive the pulse-expansion network. An expanded pulse results which is filtered before entering the first mixer, where it is upconverted to the operating frequency of the module. The expanded pulse is filtered again to block the undesired image signal and is then amplified by a transistor amplifier cascaded with a TWT to raise the signal level to that required to drive the bridge network. The bridge network is switched into either the balanced or unbalanced condition. In the balanced condition

MODULE ID: RCA 4
TAPE ID: MBL 109
FILE ID: RCA4 6/14/74 RNO

FREQ	GAIN	INSERTION PHASE ERRORS DEG
1150.0	29.97	4.47
1155.0	30.07	5.91
1160.0	30.01	2.89
1165.0	30.03	2.68
1170.0	30.41	1.43
1175.0	30.16	1.39
1180.0	30.22	1.95
1185.0	30.09	2.25
1190.0	30.34	1.12
1195.0	30.28	1.62
1200.0	30.39	1.23
1205.0	30.04	.01
1210.0	30.28	.38
1215.0	30.18	-.73
1220.0	30.27	-.51
1225.0	30.35	-.97
1230.0	30.30	-.88
1235.0	30.07	-1.20
1240.0	30.18	1.25
1245.0	29.88	-.82
1250.0	29.78	-.56
1255.0	29.99	-1.51
1260.0	29.90	-1.13
1265.0	29.88	-1.42
1270.0	29.78	.51
1275.0	29.88	-.69
1280.0	29.84	.45
1285.0	30.06	.16
1290.0	29.83	.78
1295.0	29.98	1.11
1300.0	29.74	.83
1305.0	29.99	.63
1310.0	29.80	.29
1315.0	29.94	.67
1320.0	29.59	.26
1325.0	29.85	2.80
1330.0	29.83	1.28
1335.0	29.85	2.06
1340.0	30.07	.27
1345.0	30.11	-.07
1349.9	29.91	-.35

Fig. 6b — Amplitude & phase data for RCA module #4

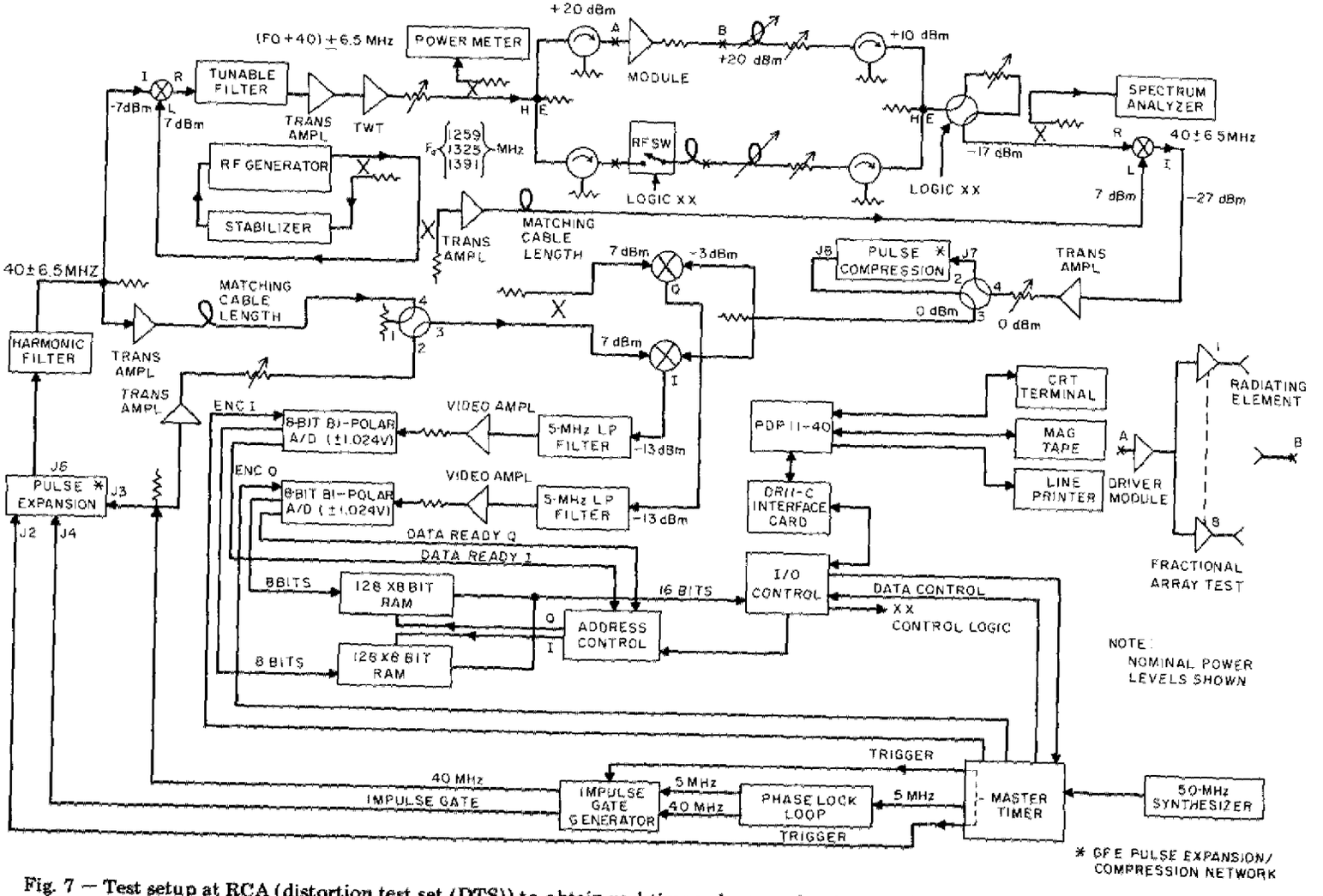

Fig. 7 — Test setup at RCA (distortion test set (DTS)) to obtain real-time pulse-to-pulse data on the distortion introduced by a module

the reference arm is switched into the circuit. It contains a cable whose length corresponds with the insertion phase of the module. The arm of the bridge which contains the module under test also contains a high-power attenuator. This is used for reducing the power level to counteract the gain of the module. Both arms of the bridge contain circulators to help reduce mismatch effects and to provide isolation between the arms. Both arms of the bridge contain line stretchers and attenuators that enable fine tuning of the bridge. The bridge is carefully balanced so that a deep null is observed at the output of the bridge. This null is obtained by observing both the power and spectral content of the bridge output. To switch to the unbalanced condition, the bridge adjustments are left untouched but the reference arm is opened and terminated in a 50-ohm load. After the switch from the balanced condition to the unbalanced condition the carrier is no longer suppressed; consequently the power level at the output of the bridge has increased by an amount equal to the depth of the null. An attenuator is used to reduce this power level back to the level corresponding to that of the balanced condition. This eliminates any effects arising from factors sensitive to power level. The output of the bridge is downconverted to the nominal 40-MHz frequency range. The downconverted signal is routed to the compression line, and then the compressed output is sampled by the A/D converters. The digital data are subsequently transferred to the magnetic tape.

All measurements taken during the experiment were of the substitution type. That is, a sequence of data was taken for a given module, the module was replaced by a suitable length of transmission line, the bridge was rebalanced, and the entire sequence of data was repeated. This technique is advantageous in that it militates against the effects of the DTS itself. However every effort was made to reduce any artifact contribution by the DTS. The two high-frequency lines between the upconversion and downconversion mixers were equalized to minimize the introduction of phase noise by the RF local oscillator. This was done when the bridge was unbalanced. The electrical lengths of the transmission lines from the two arms of the T junction to J3 of the pulse-expansion network and to the I and Q local oscillator were also equalized to minimize phase noise from the chirp generator and the 40-MHz CW local oscillator.

A signal-to-noise analysis was performed on the DTS [4]. Figure 8 is a partial diagram of the DTS showing typical signal and noise levels for the mode in which the compressed pulse is tested on transmit. All noise levels were referenced to a 5-MHz band. The lowest signal-to-noise ratio was 57 dB, and this occurred at the input to the A/D converters. The A/D converters were eight-bit devices; hence the quantization noise is about 58 dB [5] below the peak of the compressed waveform. Consequently the noise level due to the contribution of the analog circuitry is approximately that due to the quantization effects alone. A similar analysis of the other test modes shows the system analog noise level is always below or approximately equal to that of the quantization noise alone.

The dynamic range of an eight-bit A/D converter is 48 dB. In this experiment the ratio of the main-pulse level to the distortion level was of interest. The main pulse is the linear FM carrier after it has been compressed. The level of the main pulse was determined as the peak of the unbalanced response, and the level of the distortion was determined from the balanced response. The balanced response results in the suppression of the main pulse only; the distortion is not affected. The depth of the null in the balanced condition corresponds with the amount that the main pulse has been suppressed. Thus, the effective dynamic range of the experiment is increased by the depth of the null. This is about 33 dB; thus the effective dynamic range of the experiment is about 78 dB.

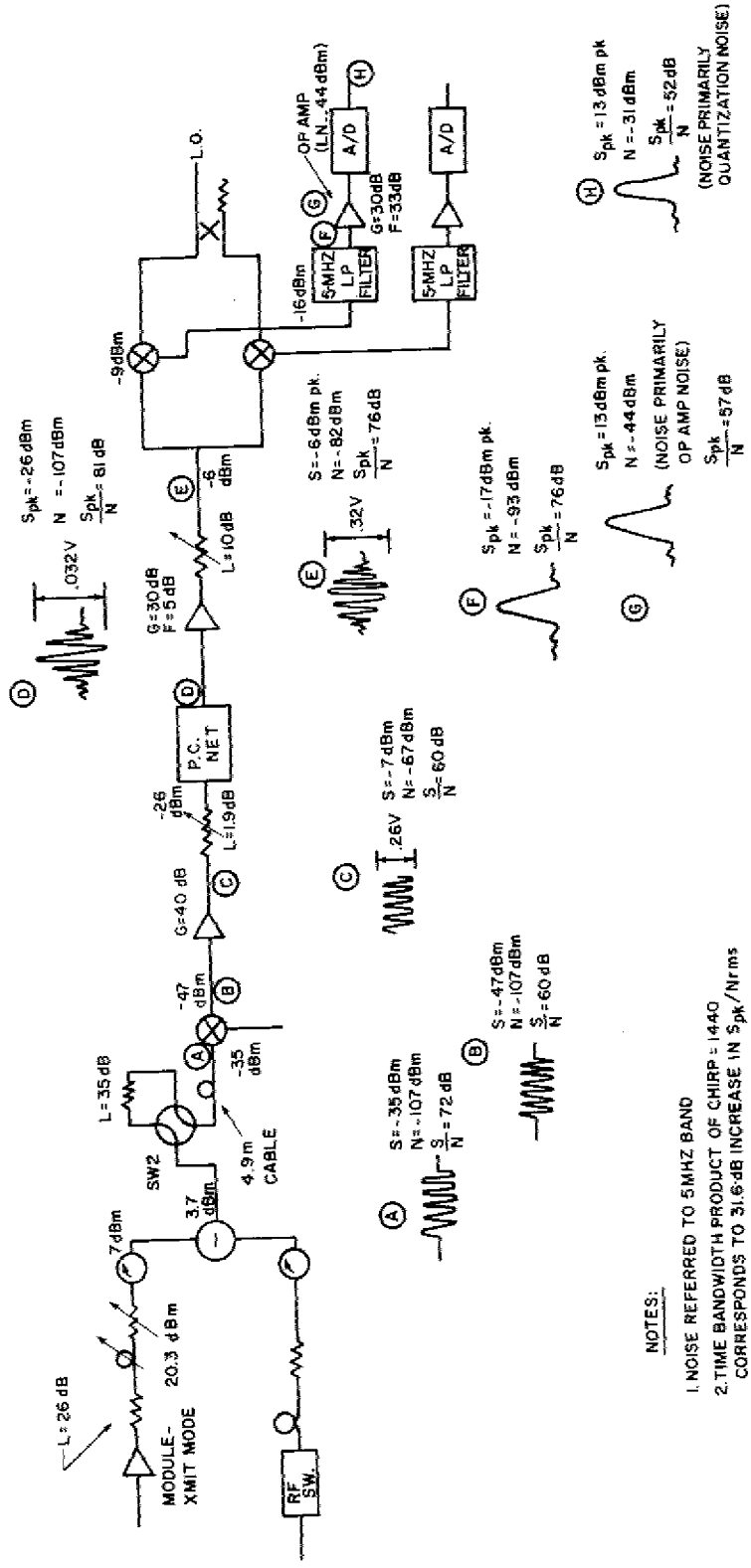

Fig. 8 — Typical signal and noise levels in the DTS when the compressed pulse is tested on transmit

Table 1 — Test Modes. The Test Modes are cycled in the following 360-mode sequence: $A_1 C_1 C_1 C_1 C_1 C_1 C_1 C_1 C_1 C_1 C_1 A_1$ repeated ten times, $B_1 D_1 D_1 D_1 D_1 D_1 D_1 D_1 D_1 D_1 D_1 B_1$ repeated ten times, and $B_2 D_2 D_2 D_2 D_2 D_2 D_2 D_2 D_2 D_2 D_2 B_2$ repeated ten times.

Test Mode	Description	Number of Samples per Pulse	Number of Pulses
A_1	Unnulled compressed pulse (measured at peak of pulse)	1	128
B_1	Unnulled uncompressed pulse	8	128
B_2	Unnulled uncompressed pulse	120	8
C_1	Nulled compressed pulse (measured at peak of pulse)	1	128
D_1	Nulled uncompressed pulse	8	128
D_2	Nulled uncompressed pulse	120	8

A particular test mode is defined by the condition of the bridge, the type of pulse measured, the number of samples per pulse, and the number of pulses recorded. Table 1 includes a listing of the various test modes. There are six test modes, but this report will analyze the data from only two of them: the unbalanced compressed-pulse mode A_1 and the balanced (or nulled) compressed-pulse mode C_1.

All data were recorded on seven-track magnetic tape. A description of the tape-file organization, record sequence, and record format is given in Tables 2 and 3. Each tape contains the data taken at one frequency for a signal module (or a single pair of modules for a cascaded configuration, with one in the transmit mode and the other in the receive mode). Each tape consists of data taken on the module as the DTS is cycled through the various test modes. A total of 360 test modes are recorded on each tape.

Seventy tapes were delivered to NRL (Table 4). Data were recorded for eight transceiver modules at three frequencies, with the modules in the transmit mode, in the receive mode, and cascaded.

These modules (Fig. 9) have a power output of 40 to 60 W peak power with an instantaneous bandwidth extending from 1259 to 1391 MHz and a power gain of approximately 27 dB in transmit. The receiver gain is approximately 27 dB with a noise figure of less than 4.5 dB and a 1-dB compression point of -25 dBm. The modules were trimmed during their manufacture to track in phase within a 14-degree rms specification for all frequencies in the design band. Table 5 gives the point-by-point phase responses of these modules.

Table 2 — Tape-File Organization (Number of files, one; file terminator, two end-of-file marks; number of records, 360; record size, variable depending on record ID (A_1, B_1, etc.); recording density, 800 bits/in. (315 bits/cm); parity, odd)

Tape Channel Number	Tape Characters
Parity	Odd parity
5	Zero or garbage
4	Zero or garbage
3	0 0 2^3 2^7 0 0 0 0 2^3 2^7 2^3 2^7 2^3 2^7 2^3 2^7
2	0 0 2^2 2^6 0 0 0 0 2^2 2^6 2^2 2^6 2^2 2^6 2^2 2^6
1	0 0 2^1 2^5 0 0 0 0 2^1 2^5 2^1 2^5 2^1 2^5 2^1 2^5
0	0 0 2^0 2^4 0 0 0 0 2^0 2^4 2^0 2^4 2^0 2^4 2^0 2^4
	HEADER: ID; I Q I Q

Data Processing

The tapes generated during the course of the measurements underwent further processing at NRL. This processing included making a copy of the contractor-supplied tapes. This was done to protect the original data and, at the same time, convert the data from the original hyperdensity (315-bit/cm) format to the high-density (219-bit/cm) format. This conversion was necessary to prevent scheduling problems and for economical handling of the tapes, since the available hyperdensity data-processing capability was limited. The final processing step, prior to the analysis, was to depack the data and to convert it to a format of one computer word per data word. This made the data more suitable for repetitive analysis.

Summary of Experimental Procedure

The experimental program was carried out in two phases: a feasibility phase and a measurement phase. The feasibility phase was concerned with the development of a suitable experimental apparatus with a sensitivity sufficient to expose the time-sidelobe effects induced by the module distortions. The measurement phase was originally conceived to be an implementation of the earlier experimental apparatus along with some recording equipment to permit looking at the individual pulses on a real-time pulse-to-pulse basis. The measurement phase turned out to be significantly more involved due to problems which became apparent after the recording capability was established.

Table 3 — Tape-Record Formats

Record	Record ID	Size		Format	
		Tape Characters	Bytes	Header Characters	Data Characters
A_1	1	520	260	8	512
B_1	2	4104	2052	8	4096
B_2	3	3848	1924	8	3840
C_1	4	520	260	8	512
D_1	5	4104	2052	8	4096
D_2	6	3848	1924	8	3840

Tape Record Sequence:

Records 1 through 120 contain Test Sequence 1, repeated 10 times. A1C1C1C1C1C1C1C1C1C1C1A1... (Ten times)

Records 121 through 240 contain Test Sequence 2, repeated 10 times. B1D1D1D1D1D1D1D1D1D1D1B1... (Ten times)

Records 241 through 360 contain Test Sequence 3 repeated 10 times. B2D2D2D2D2D2D2D2D2D2D2B2... (Ten times)

Records 361 & 362 are end of file marks.

The modules which were the subject of the investigation operated at 1250 to 1400 MHz. The pulse expansion/compression network which generated the expanded pulse and compressed the output signal from the bridge network used surface-wave dispersive delay lines and operated at 40 MHz. The instantaneous bandwidth of the expanded chirp pulse was 13 MHz.

The test configurations used during the two phases of the experiment are shown in Figs. 3 and 7. They both operated in essentially the same manner. A mixer was used to upconvert the frequency range of the expanded pulse to the module operating frequency. The signal was then filtered to remove the undesired sideband. This signal was used to excite the bridge network. Upon emerging from the bridge, the energy due to the pulse was translated back down to the nominal 40-MHz frequency band. Finally the energy was routed through the compression network and was compressed.

In the analysis of the experiments certain simplifying assumptions regarding the test setup are made. These are that the expansion and compression operations undo one another perfectly and that the frequency translations have no net effect. These assumptions, which are based on the designed functioning of the components involved, are believed to be valid, particularly since the measurements made were of the substitution type. A module's response was measured and then an appropriate length of transmission line substituted for the module and the process was repeated. Thus the test setup was in a sense calibrated.

Table 4 — Phase-Two Tapes Delivered to NRL

Tape No.	Module No.	Freq. (MHz)	Mode	Attenuation (dB)		Tape No.	Module No.	Freq. (MHz)	Mode	Attenuation (dB)	
				A, C	B, D					A, C	B, D
00	—*	1326	—	—	—	38	88m	1266	Rcv	39.0	26
1	—†	1326	Xmit	39	30	39	81m	1266	Rcv	39	27
2	37m	1326	Xmit	28	17	41	—‡	1326	Rcv	35	28
3	18m	1326	Xmit	36	20	42	37m	1326	Rcv	55	25
4	47m	1326	Xmit	33	15	43	18m	1326	Rcv	42	34
5	48m	1326	Xmit	35	23	44	47m	1326	Rcv	52	35
6	43m	1326	Xmit	32.5	17	45	48m	1326	Rcv	51	36.5
7	46m	1326	Xmit	34.0	17.5	46	43m	1326	Rcv	50	44
8	88m	1326	Xmit	32	18.0	47	46m	1326	Rcv	51	32
9	81m	1326	Xmit	31	13.0	48	88m	1326	Rcv	45	32
11	—†	1266	Xmit	35	28	49	81m	1326	Rcv	45	30
12	37m	1266	Xmit	31	14	51	—‡	1386	Rcv	40	28
13	18m	1266	Xmit	32	18	52	37m	1386	Rcv	52	39
14	47m	1266	Xmit	25	13	53	18m	1386	Rcv	42	31
15	48m	1266	Xmit	26	19	54	47m	1386	Rcv	45	36
16	43m	1266	Xmit	25	11	55	48m	1386	Rcv	47	28
17	46m	1266	Xmit	36	18	56	43m	1386	Rcv	40	36
18	88m	1266	Xmit	33	21	57	46m	1386	Rcv	39	34
19	81m	1266	Xmit	31	18	58	88m	1386	Rcv	51	35
21	—†	1383	Xmit	37	24 A_1	59	81m	1386	Rcv	46	35
22	37m	1383	Xmit	35	14 A_1	61	81m-48m	1266	Xmit-Rcv	31	27
23	18m	1383	Xmit	33	17.5	62	47m-88m	1266	Xmit-Rcv	34	27
24	47m	1383	Xmit	32.5	16	63	46m-18m	1266	Xmit-Rcv	35	20
25	48m	1383	Xmit	31	17	64	43m-37m	1266	Xmit-Rcv	36	20
26	43m	1383	Xmit	28	15	65	—ϕ	1266	Xmit-Rcv	37	25
27	46m	1383	Xmit	32	11	66	81m-48m	1326	Xmit-Rcv	41	21
28	88m	1383	Xmit	29	18	67	47m-88m	1326	Xmit-Rcv	36	20
29	81m	1383	Xmit	29	16	68	46m-18m	1326	Xmit-Rcv	37	23
31	—‡	1266	Rcv	40	25	69	43m-37m	1326	Xmit-Rcv	32	19
32	37m	1266	Rcv	55.5	29	70	—ϕ	1326	Xmit-Rcv	41	30
33	18m	1266	Rcv	48.0	29	71	81m-48m	1386	Xmit-Rcv	35	16
34	47m	1266	Rcv	47.0	29	72	47m-88m	1386	Xmit-Rcv	35	16
35	48m	1266	Rcv	45.0	29	73	46m-18m	1386	Xmit-Rcv	37	11
36	43m	1266	Rcv	45.0	28	74	43m-37m	1386	Xmit-Rcv	38	15
37	46m	1266	Rcv	43.0	26	75	—ϕ	1386	Xmit-Rcv	40	33

*Ref.; Lo on, RF off.
†264.5-cm ref. cable (module-37 length).
‡133-cm ref. cable length.
ϕ264.5-cm and 133-cm ref. cable lengths.

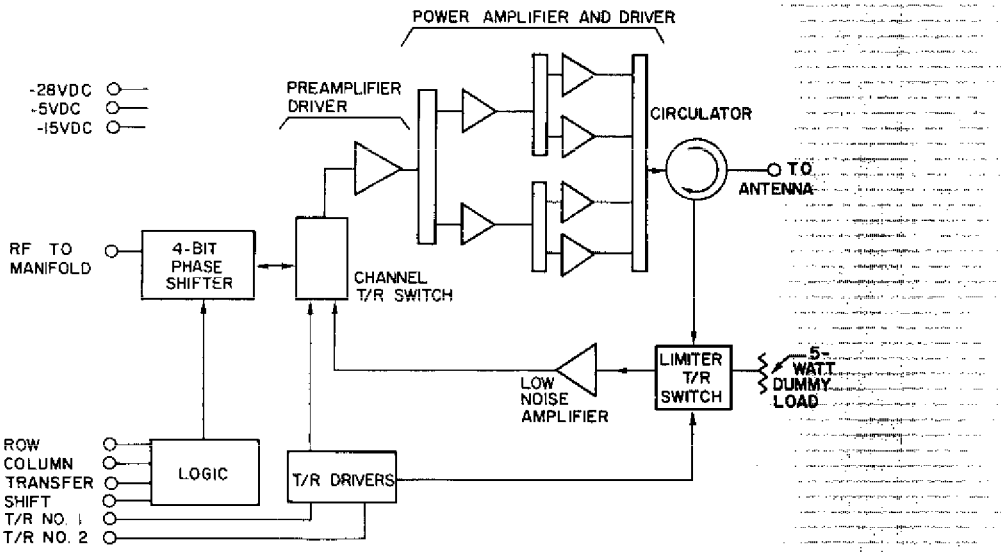

Fig. 9 — Transmit/receiver module tested

Table 5 — Phase Data for the Modules Tested

Module No.	Phase (deg)										
	1259 MHz	1272 MHz	1285 MHz	1298 MHz	1311 MHz	1324 MHz	1337 MHz	1350 MHz	1363 MHz	1376 MHz	1389 MHz
Transmit Mode											
18m	396.6	388.0	390.6	393.7	398.5	403.2	407.1	396.9	398.0	396.0	397.0
37m	401.6	398.1	390.6	401.1	405.1	401.2	398.4	401.6	403.9	409.3	411.1
46m	375.1	381.6	392.2	396.1	392.6	398.5	402.4	405.7	408.6	411.4	416.0
43m	385.3	385.4	398.4	403.7	403.8	399.2	398.4	402.6	410.3	413.1	419.2
47m	353.1	360.0	371.4	380.1	384.1	384.0	383.7	386.8	387.8	392.2	400.4
48m	375.2	381.0	382.7	386.5	392.0	393.2	392.4	396.9	402.1	417.6	426.1
81m	393.2	397.1	402.6	405.0	404.8	403.8	407.8	403.7	415.7	423.1	428.1
88m	376.2	359.7	367.9	381.6	385.2	388.6	392.8	392.2	404.8	403.9	408.4
Receive Mode											
18m	24.	-7.5	-39.3	-72.4	-104.3	-136.4	-168.5	-200.2	-228.8	-261.2	-291.8
37m	17.1	-13.4	-43.4	-74.5	-104.3	-134.2	-164.3	-194.4	-222.1	-254.1	-285.
45m	16.9	-13.7	-44.2	-76.4	-107.3	-188.5	-169.6	-199.6	-226.6	-258.3	-287.2
43m	16.4	-14.3	-44.8	-76.7	-107.1	-137.5	-167.5	-196.8	-225.4	-254.6	-283.6
47m	14.5	-16.2	-46.4	-77.5	-107.2	-137.1	-167.2	-197.4	-227.1	-257.5	-287.8
48m	19.	-10.4	-39.7	-70.5	-99.8	-128.7	-158.1	-186.5	-214.7	-244.	-273.4
81m	8.5	-21.	-49.7	-79.8	-108.9	-138.2	-167.8	-197.6	-225.7	-257.6	-287.6
88m	22.	-8.2	-38.6	-70.1	-100.3	-130.3	-160.4	-189.9	-216.7	-247.7	-277.

ANALYSIS

The analysis is presented in the following two subsections. The first subsection specifically addresses those aspects of the experiment concerned with the distortion induced by the modules. An analysis of the bridge network/pulse compression filter is presented. The time-domain representation of the network response is discussed for various forms of distortion. The second subsection addresses stability on both an intrapulse and interpulse basis. A spectral analysis is performed of the data generated during the second phase of the experiment with respect to the pulse-to-pulse variation.

Time-Sidelobe Analysis

A schematic of a simplified version of the experimental setup in either Fig. 3 or Fig. 7 is given in Fig. 10a. The heart of the experiment is the bridge or cancellation network. During the measurement, the residue or output of the bridge network is fed into a pulse-compression line. The residue as it will appear at the output of the pulse-compression line is analyzed using the paired-echo approach [1,2,6].

One arm of the bridge consists of the module or device under test, an attenuator to reduce the power output of the module, and a phase shifter to permit fine tuning of the bridge. The other arm of the bridge serves as a reference arm and contains an attenuator, a phase shifter, and a transmission line whose length has been chosen to correspond to the time delay provided by the module. The transfer function of the entire arm containing the module as it affects the video frequency modulation will be represented as $H_1(\omega)$, and the transfer function of the entire reference arm will be represented as $H_2(\omega)$, as shown in Fig. 10b. Then the transfer function of the bridge network for the balanced or nulled condition can be expressed as

$$E_o(\omega) = E_i H_o(\omega) = E_i \frac{1}{2} [H_1(\omega) - H_2(\omega)],$$

where

$E_o = E_o(\omega)$ = output signal from the bridge network,

$E_i = E_i(\omega)$ = input signal to the bridge network,

$H_o(\omega)$ = transfer function of the bridge network (video frequency equivalent).

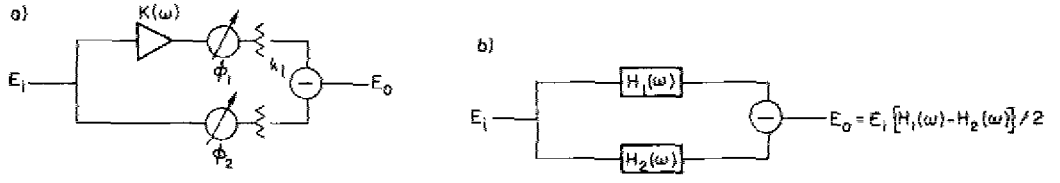

(a) Physical model (b) Analytical model

Fig. 10 — Simplified version of either Fig. 3 or Fig. 7

The transfer function of the arm containing the module can be written as

$$H_1(\omega) = K(\omega)e^{j\phi(\omega)},$$

where

$$\phi(\omega) = \phi + B(\omega)$$

and

$$K(\omega) = A(\omega)e^{-jb_0\omega}.$$

Expressing $A(\omega)$ and $B(\omega)$ in Fourier series representations yields

$$A(\omega) = a_0 + \sum_{n=1}^{\infty} a_n \cos nc\omega$$

and

$$B(\omega) = \sum_{m=1}^{\infty} b_m \sin mc'\omega.$$

If these expressions are approximated by their first harmonic term ($n = 1$), and these approximations substituted into the expression for $H_1(\omega)$, then the expression becomes

$$H_1(\omega) \approx (a_0 + a_1 \cos c\omega)e^{j[-b_0\omega + b_1 \sin(c'\omega) + \phi]}.$$

The term $e^{jb_1 \sin c'\omega}$ can be expanded using a formula from the theory of Bessel functions to the first order, for small b_1:

$$e^{jb_1 \sin c'\omega} = 1 + jb_1 \sin c'\omega.$$

Substitution of this expansion into the expression for $H_1(\omega)$ yields

$$H_1(\omega) \approx [a_0(1 + jb_1 \sin c'\omega) + a_1 \cos c\omega(1 + jb_1 \sin c'\omega)]\, e^{j(-b_0\omega + \phi)}.$$

If the term involving the cross product of the small quantities a_1 and b_1 is dropped, then

$$H_1(\omega) \approx (a_0 + a_1 \cos c\omega + ja_0 b_1 \sin c'\omega)e^{j(-b_0\omega + \phi)}$$

No assumption has been made regarding the size of a_0 or b_0. Cook and Bernfield [1] have shown that for phase distortions less than 0.5 radian it is permissible to ignore cross-product terms and treat the amplitude and phase distortions as independent. The total phase distortion in the module is on the order of ±15 degrees over an operating bandwidth of a couple of hundred megahertz, significantly less than the value set by Cook and Bernfield as an upper limit. Here the analysis is concerned with the instantaneous bandwidth of the video input signal (13 MHz). Thus the preceding approximation which ignores the cross-product terms should be acceptable. This approximation can be rewritten as

$$H_1(\omega) \approx a_0 e^{j(-b_0\omega+\phi)}\left(1 + \frac{a_1}{a_0}\cos c\omega + jb_1 \sin c'\omega\right).$$

Since the reference arm contains only a length of transmission line and an attenuator, its transfer function may be written as

$$H_2(\omega) = a_0' e^{j(-b_0'\omega+\phi')},$$

where

a_0' = total attenuation in the reference arm,

$b_0'\omega$ = is the linear phase shift characteristic of transmission line,

ϕ' = a constant-phase term.

Then the expression for E_o reduces to

$$E_o = \frac{1}{2} E_i a_o e^{j(-b_o\omega+\phi)}\left\{1 + \frac{a_1}{a_0}\cos c\omega + jb_1 \sin c'\omega - \frac{a_0'}{a_0} e^{j[\omega(b_o-b_o')+\phi-\phi']}\right\}.$$

Evidently the balanced condition is achieved when $a_o = a_o'$, $b_o = b_o'$, and $\phi = \phi'$. Thus the output in the balanced condition reduces to

$$E_0 = \frac{1}{2} E_i a_o e^{j(-b_o\omega+\phi)}\left(\frac{a_1}{a_0}\cos c\omega + jb_1 \sin c'\omega\right).$$

This expression for E_o describes the transform of the output of the bridge network. The output of the bridge then can be thought of as the input to the pulse-compression filter. In the experiment the compression-filter output was viewed as a function of time.

To provide some intuitive feel for the nature of the output of the pulse-compression filter, E_o will be further examined. As expressed by the preceding equation, E_o can be described as a product of the input E_i, a function $H_u(\omega)$ which has a constant-amplitude characteristic and a phase characteristic which is proportional to frequency, and a function which will be referred to as the distortion function $H_d(\omega)$. This is appropriate, since Goldman [2, pp. 68-70] has shown that the constant-amplitude, linear-phase function produces a change in amplitude scale and a time delay only. In other words it is free of distortion. Any distortion then can be attributed to the function $H_d(\omega)$. Thus

$$E_o = E_i H_u(\omega) H_d(\omega),$$

where

$$H_u(\omega) = \frac{1}{2} a_o e^{j(-b_o+\phi)}$$

and

$$H_d(\omega) = \frac{a_1}{a_0} \cos c\omega + jb_1 \sin c'\omega.$$

The distortion function $H_d(\omega)$ will be analyzed in the time domain in terms of paired-echo concepts, following an analysis similar to that of Cook and Bernfield [1] and of Goldman [2].

It will be instructive to investigate a few simple cases to see how the phase and amplitude distortions affect the waveform at the output of the compression filter. The bridge network, including the module being tested, will be considered as a distortion filter with a transfer function $H(\omega) = H_u(\omega)H_d(\omega)$. The input spectrum to the bridge network is $E_i(\omega)$ and the output spectrum is $E_i(\omega)H(\omega)$, so in the time domain

$$e_u(t) = \frac{1}{2\pi} \int_{-\infty}^{\infty} E_u(\omega)e^{j\omega t}\, d\omega = \frac{1}{2}\, a_0 e_i(t - b_0)$$

where

$$E_u = E_i H_u(\omega) \text{ and } e_i(t) = \frac{1}{2\pi} \int_{-\infty}^{\infty} E_i(\omega)e^{j\omega t}\, d\omega.$$

The distorted output time function is

$$e_d(t) = \frac{1}{2\pi} \int_{-\infty}^{\infty} E_u(\omega)H_d(\omega)e^{j\omega t}\, d\omega$$

or, with the full expression for $H_d(\omega)$ substituted,

$$e_d(t) = \frac{1}{2\pi} \int_{-\infty}^{\infty} E_u(\omega)\left(\frac{a_1}{a_0} \cos c\omega + jb_1 \sin c'\omega\right)e^{j\omega t}\, d\omega,$$

which is a general expression for the distorted output time function when first-order amplitude and phase distortion are both present.

The case in which only amplitude distortion is present corresponds to setting $b_1 = 0$. Then if the cosine term is rewritten in terms of complex exponentials as

$$\frac{a_1}{a_0} \cos c\omega = \frac{a_1}{a_0}\left(\frac{e^{jc\omega} + e^{-jc\omega}}{2}\right),$$

the expression for the distorted output signal becomes, after the indicated integration,

$$2e_d(t) = \frac{a_1}{a_0}\ [e_u(t+c) + e_u(t-c)] = \frac{a_1}{2}\ [e_i(t'+c) + e_i(t'-c)],$$

where $t' = t - b_0$. The first and second terms of the distorted output signal represent advanced-in-time and delayed-in-time replicas of the undistorted signal $e_u(t)$, weighted by a factor of $a_1/2a_0$. The replicas of the undistorted signal are symmetrically advanced and delayed from the undistorted signal by a time interval c, as shown in Fig. 11a, and are commonly referred to as *paired echoes.*

The situation in which only phase distortion is present corresponds to setting $a_1 = 0$. Substitution of this assumption into the equation for the distortion yields

$$2e_d(t) = \frac{1}{2\pi} \int_{-\infty}^{\infty} E_u(\omega)(jb_1 \sin c'\omega)e^{j\omega t}\, d\omega,$$

which, after the integrand is expanded in terms of exponentials and the indicated integration is performed, becomes

$$2e_d(t) = b_1[e_u(t+c') - e_u(t-c')] = \frac{a_0 b_1}{2}\ [e_i(t'+c') - e_i(t'-c')],$$

where $t' = t - b_0$. This expression for the distortion is valid for relatively small phase errors ($b_1 < 0.5$ radian) and is quite similar to the solution obtained for the case in which only amplitude distortion is present except that the echo terms have opposite polarity (Fig. 11b).

For small amplitude and phase distortion the individual components of the distortion function will contribute an independent set of paired echoes, so that the effect of the composite amplitude and phase distortion is described by

$$2e_d(t) = \frac{a_0 b_1}{2}\ [e_i(t'+c') - e_i(t'-c')] + \frac{a_1}{2}\ [e_i(t'+c) + e_i(t'-c)].$$

This equation, as depicted in Fig. 11c, shows that the effect of a composite amplitude and phase distortion is the generation of a number of echoes of varying magnitude, some of which will be negative. The spacing between the paired signals will depend only on the number of cycles of the distortion function over the duration of the uncompressed pulse. For example, if there are five cycles of the distortion function over the nominal bandwidth, then the first set of paired echoes will be approximately five compressed pulse widths removed from the center pulse location. The nominal bandwidth of a chirp pulse is approximately $2D/T$, where T is the length of the uncompressed pulse and D is the dispersion factor or compression ratio. Conversely, if the distortion function is a slowly changing function over the nominal band, the paired echoes may substantially overlap with the undistorted signal output or center pulse. When this happens, it is possible to

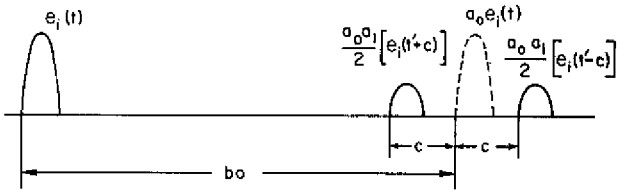

(a) Effect of amplitude distortion only

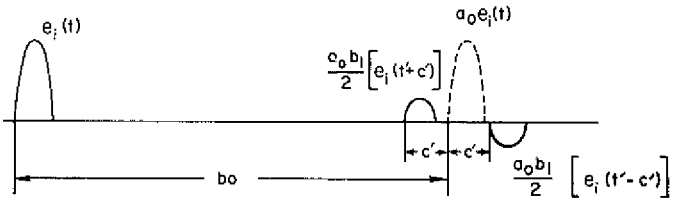

(b) Effect of phase distortion only

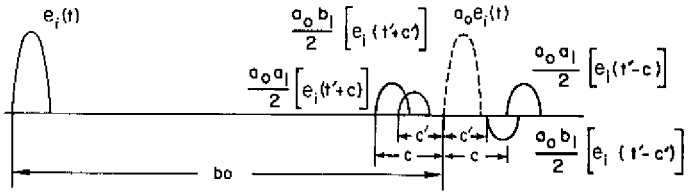

(c) Effect of both a small amplitude distortion and a small phase distortion

Fig. 11 — Effect of phase and amplitude distortions on the waveform at the output of the compression filter. (Because balancing of the bridge in this experiment suppresses the undistorted signal at the output of the compression line, the undistorted signal is dashed.)

obtain various patterns of cancellation and reinforcement in the composite waveform, depending on the coefficients of the Fourier expansion representing the phase and amplitude distortion function.

Spectral Analysis of Pulse-to-Pulse Variations

During the second phase of the experiment the measurement effort included the monitoring and recording of the output of the pulse-compression filter for both the balanced and unbalanced conditions of the bridge circuit.

In the balanced condition the reference arm of the bridge is adjusted to obtain a maximum depth of the null. The undistorted center lobe of the time-domain response is then canceled out by the bridge network. The nulling scheme increases the sensitivity or effective dynamic range of the experiment and exposes the residue which results in

distortion-induced time sidelobes. The waveform at the output of the compression filter is monitored on a pulse-to-pulse basis for consecutive pulse trains, each of which is long in terms of the processing cycle.

In the unbalanced condition the arm of the bridge containing the module remains identical with the arm in the corresponding balanced-condition measurement but the reference arm is opened and terminated in a 50-ohm load. This operation has the effect of removing the reference arm, and no cancellation of the carrier occurs. Therefore the output of the compression filter is the normal time-domain response as it would occur in a typical radar application. The output of the compression filter was monitored as for the nulled case.

The characteristics of the input signal and of the pulse train were essentially dictated by the AEW application and, to some extent, by limitations of the equipment used in the experiment. As in the first-phase measurements, the input signal was the expanded pulse generated by the expansion-compression line. This expanded pulse is a linear FM signal with a rectangular modulation envelope 120 μs long. The nominal bandwidth is 13 MHz about a center frequency of 40 MHz. The pulse repetition frequency (PRF) was chosen to be 300 Hz, and the frequency was synchronized with and derived from a highly accurate and stable 5-MHz master timer. The length of the pulse train was chosen to be long compared with the radar processing cycle, yet not so large as to exceed the real-time recording capability of the equipment used in the experiment. Current estimates indicate that a processing cycle consisting of 16 to 24 pulses will be sufficient for future AEW applications. The pulse trains were necessarily recorded in real time. Since the recording equipment could not transfer the data to magnetic tape at this rapid rate, it was necessary to use a random-access memory as an interim storage. The PDP 11-40 computer then transferred the data onto magnetic tape at a reduced data rate. A pulse train containing 128 pulses was chosen based on the preceding considerations.

Both in-phase (I) and quadrature (Q) samples were taken at a rate equal to the PRF. Therefore the sampling rate was 300 complex samples per second. This is consistent with the requirements set forth by the sampling theorem of Papoulis [7,p.119] for a total bandwidth of 300 Hz. The set of data from a pulse train consisted of 256 samples, of which one group of 128 samples consisted of I samples and the other group of 128 consisted of Q samples. The I and Q samples were made up of 128 complex values, each of which corresponded with the output of the compression filter for one of the 128 pulses forming the pulse train. These complex values were fed into a discrete Fourier transform (DFT), which derived the spectrum in the frequency domain. The magnitude of this spectrum was then squared to obtain the power-spectrum representation. Many pulse trains were available for each test condition. A more representative power spectrum was generated by performing the DFT on ten pulse-trains and averaging the power spectra at each frequency.

A computer program was written to perform the preceding operations and also to compute the mean and the standard deviation of the I and Q samples. This program will be referred to as the spectral-analysis program. A sample set of input data for the program is given in Fig. 12. This corresponds with the data for a single pulse-train and was taken when module 37m was under test. The output of the computer program for this module at 1326 MHz is given in Fig. 13. The output includes the mean value and standard deviation of the I and Q data and a plot of the spectral density.

INPUT TO FFT

37.0000	164.0000	46.0000	173.0000	43.0000	172.0000	47.0000	175.0000
42.0000	170.0000	41.0000	170.0000	45.0000	173.0000	42.0000	171.0000
42.0000	170.0000	46.0000	173.0000	41.0000	170.0000	47.0000	175.0000
38.0000	166.0000	47.0000	175.0000	45.0000	173.0000	40.0000	169.0000
42.0000	170.0000	42.0000	171.0000	46.0000	175.0000	46.0000	174.0000
37.0000	165.0000	46.0000	173.0000	42.0000	171.0000	47.0000	175.0000
42.0000	170.0000	41.0000	170.0000	47.0000	174.0000	42.0000	171.0000
42.0000	170.0000	46.0000	174.0000	41.0000	170.0000	47.0000	175.0000
38.0000	166.0000	47.0000	175.0000	46.0000	174.0000	41.0000	170.0000
41.0000	168.0000	42.0000	172.0000	46.0000	175.0000	46.0000	175.0000
36.0000	165.0000	45.0000	173.0000	42.0000	172.0000	47.0000	175.0000
42.0000	170.0000	40.0000	170.0000	45.0000	173.0000	41.0000	171.0000
42.0000	170.0000	45.0000	173.0000	41.0000	170.0000	45.0000	174.0000
37.0000	166.0000	46.0000	175.0000	46.0000	175.0000	39.0000	169.0000
44.0000	172.0000	37.0000	167.0000	46.0000	175.0000	45.0000	174.0000
39.0000	169.0000	41.0000	169.0000	42.0000	172.0000	47.0000	176.0000
45.0000	175.0000	35.0000	164.0000	45.0000	173.0000	41.0000	172.0000
46.0000	175.0000	41.0000	169.0000	40.0000	170.0000	45.0000	173.0000
41.0000	171.0000	42.0000	172.0000	46.0000	175.0000	40.0000	169.0000
46.0000	173.0000	37.0000	167.0000	47.0000	176.0000	45.0000	174.0000
40.0000	169.0000	41.0000	169.0000	42.0000	171.0000	46.0000	175.0000
46.0000	175.0000	36.0000	164.0000	45.0000	173.0000	42.0000	171.0000
46.0000	175.0000	41.0000	170.0000	41.0000	170.0000	44.0000	173.0000
41.0000	172.0000	42.0000	170.0000	45.0000	174.0000	40.0000	170.0000
45.0000	174.0000	37.0000	166.0000	46.0000	175.0000	45.0000	173.0000
40.0000	169.0000	41.0000	169.0000	42.0000	171.0000	46.0000	175.0000
45.0000	175.0000	36.0000	165.0000	45.0000	173.0000	41.0000	172.0000
46.0000	175.0000	41.0000	169.0000	41.0000	170.0000	45.0000	173.0000
41.0000	172.0000	42.0000	171.0000	45.0000	174.0000	40.0000	170.0000
46.0000	174.0000	37.0000	166.0000	46.0000	175.0000	45.0000	174.0000
40.0000	170.0000	41.0000	170.0000	41.0000	172.0000	46.0000	175.0000
45.0000	175.0000	36.0000	165.0000	45.0000	173.0000	41.0000	172.0000

Fig. 12 — Sample set of input data for the spectral analysis program

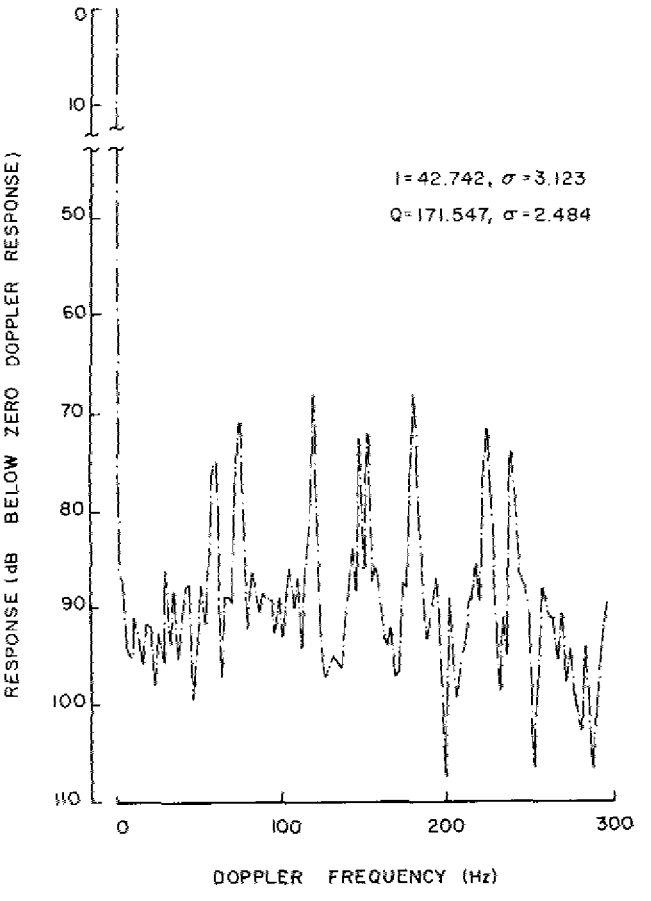

Fig. 13 — Spectral response of module 37m (transmit, 1326 MHz), computed and plotted by the computer program using the input data of Fig. 12.

DISCUSSION OF THE SPECTRAL DENSITY

The characteristics of the received signal as it appears at the input to the radar signal processor is of prime importance in an AEW system. The characteristics of this signal are affected by a multitude of factors including effects of the target, of the system itself, and of the environment in which the system must function. Techniques have been developed to aid the system in separating the contribution due to each effect. Problems arise when the system is unable to distinguish these contributions from one another. The system effectiveness can be severely limited if the effects normally associated with the target are produced by the operation of the system itself.

In the case of the spectral density it was assumed that all signals which appear in the doppler-frequency domain are induced by the target. If spurious sidebands or signals are present which are not target induced, then some means must be used to discriminate against these signals. If the spurious sidebands are much smaller than the carrier, then the discrimination could be based on the power content. If the spurious sideband occurs at a frequency other than that of interest, then this could be the basis for distinguishing

one signal from the other. But if the signal appears in the doppler domain at a level which corresponds to a target size of interest for that range cell, then the detection capability of system must suffer, because the signal will be represented as a target.

In the second phase of the experiment, data were taken to permit the calculation of the spectral density of various combinations of modules. The combinations measured were the module in the transmit mode, the module in the receive mode, and two modules in cascade, one in the transmit mode and the other in the receive mode.

A plot of the spectra of module 37m with the bridge circuit in the balanced condition was given in Fig. 13. The abscissa corresponds to the doppler frequency range, and extends from 0 Hz out to 300 Hz. The frequency resolution is 300/128 Hz, or 2.34 Hz. The ordinate corresponds to the relative level of the spectral response. The peak of this spectral response occurs at zero doppler frequency. This is a measure of the mean or normal value of the compressed pulse of the linear FM signal. In the absence of pulse to pulse variations the spectral response would be limited to an impulse at zero doppler frequency. The response falls sharply from its zero-doppler value to a value more than 65 dB down relative to the mean sample power of canceled output, or approximately 95 dB down relative to the signal (30 dB being the nominal difference in the power levels for the balanced and unbalanced conditions of the bridge). A series of spectral peaks which rise from this low level up some 30 dB to the level of -65 dB relative to the signal carrier.

Figure 14 is a repeat of the spectrum of module 37m except that the spectra have been averaged over ten pulse trains. Each of the ten pulse trains consists of 128 pulses; thus the spectra in Fig. 14 and subsequent figures are averaged over 1280 pulses. As expected, the averaging operation tends to smooth out the response and therefore to make the frequencies at which the module's contribution is significant more visible. All subsequent plots averaged over ten pulse trains.

Peaks also occur at the power-supply frequency and at all of its harmonics. The peaks occurred even though high-quality laboratory power supplies were used for all tests and special care was taken to prevent grounding problems. Thus the spectral-density data must be viewed with this in mind. It is an open question at this time whether the peaks attributed to the power-supply ripple and its harmonics could be reduced by improved filtering etc. But it is doubtful that in practice much improvement would be achieved in an airborne system.

No attempt will be made to present all the data taken during the experiment; however Figs. 15 through 25 include representative plots of module spectra at the low, mid, and high RF frequencies for each of the individual test configurations.

Figure 15a is a plot of the averaged spectra of module 37m in the transmit mode at 1326 MHz for the nulled and unnulled test conditions. The curve labeled "C_1, nulled" pertains to the module response when the bridge network has been adjusted to a nulled or balanced condition. The curve labeled "A_1, unnulled" is the corresponding result for the unnulled or unbalanced condition. The curve designated "calibration" pertains to the response of the bridge network when nulled with a length of transmission line substituted for the module. The "calibration" curve, in effect, is the contribution of the test set to the measured spectra. The "calibration" curve sets a lower limit on the dynamic range of the experiment. Figure 15b is a similar plot of module 47m.

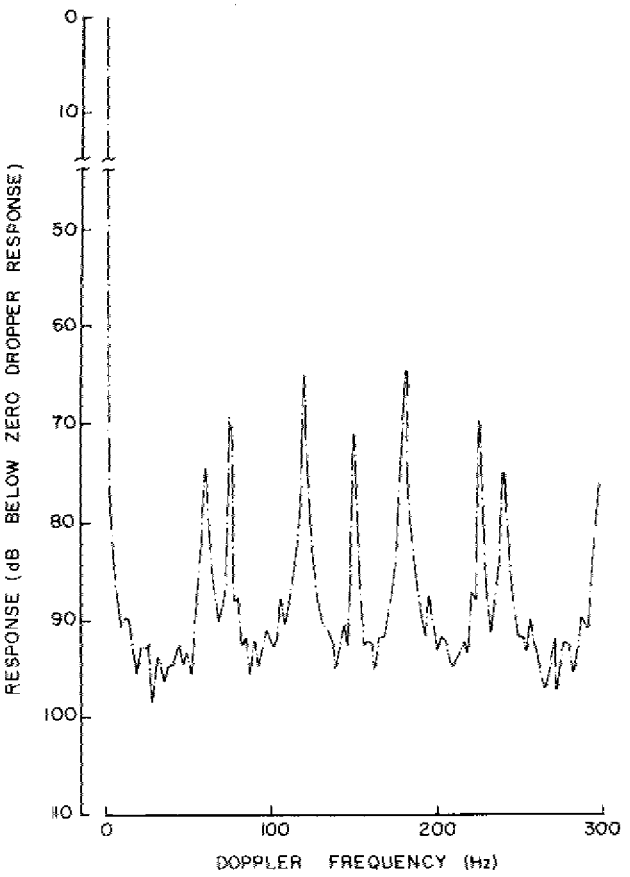

Fig. 14 — Spectral response of module 37m (transmit, 1326 MHz, averaged over ten pulse trains)

Figure 16 shows the averaged nulled response for modules 18m, 37m, 43m, 47m, 48m, 81m, and 88m in the transmit mode at 1326 MHz. Figure 16 also includes the calibration curve and an indication of the cancellation ratio that is currently achieved. The calibration spectra curve is substantially below that of the spectra recorded for the modules. This indicates that the measurement was performed within the dynamic range of the test set and that the contribution of the test set to the measured spectra is minimal. A similar calibration curve is shown on all subsequent plots. The typical cancellation ratio or improvement factor in present-day AEW systems is on the order of 60 dB. The plot shows that the spectra measured for the modules is below this 60-dB figure at all doppler frequencies. With the exception of the power supply related frequencies (60 Hz or multiples thereof) and sharp spikes at approximately 80, 150, and 220 Hz, the general level of the module induced spectra lie more than 80 dB below the zero-doppler response.

Figure 17 shows the spectra of modules 47m, 48m, and 88m in the transmit mode at 1266 MHz. (Module 81m is not included here due to a bad tape which prevented processing of data.)

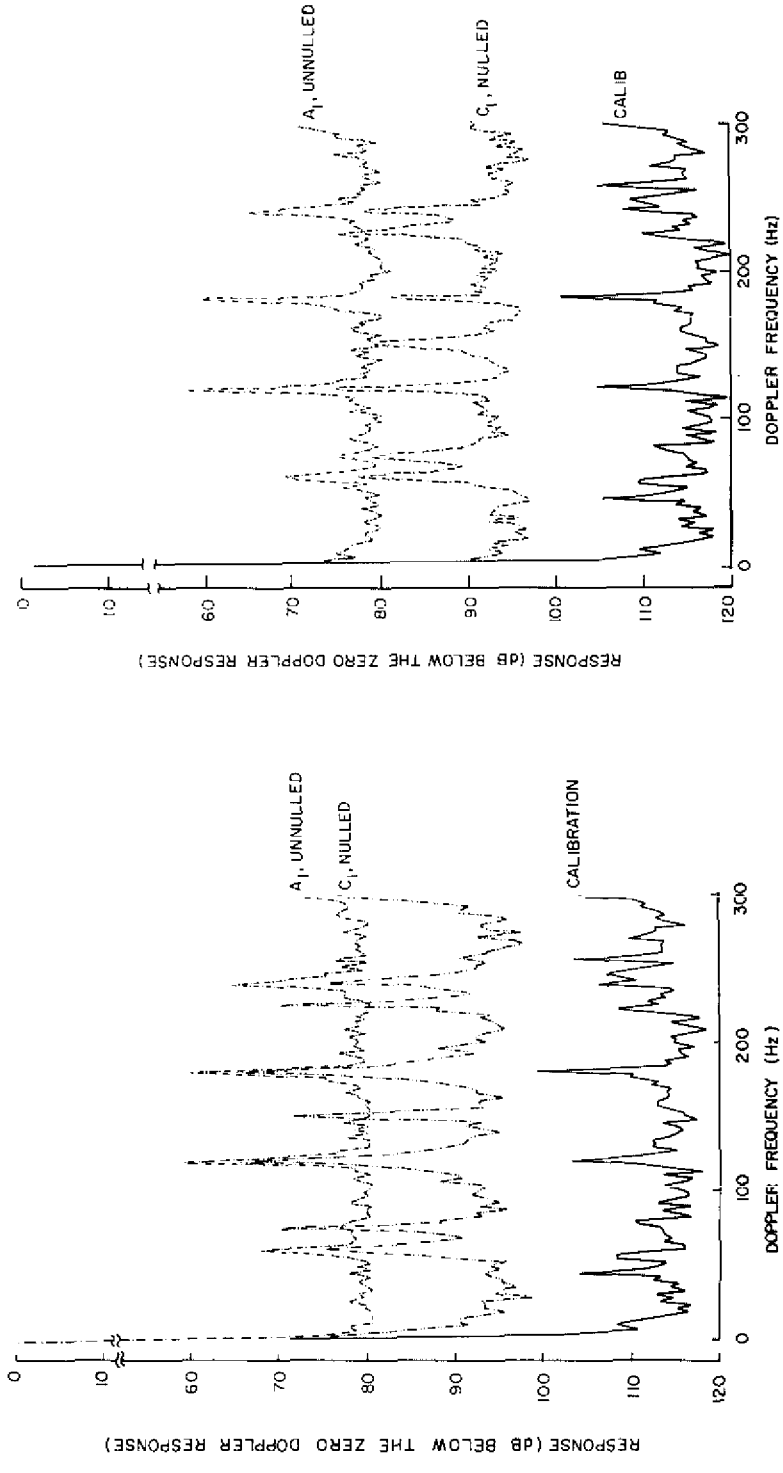

(a) Module 37m (b) Module 47m

Fig. 15 — Spectral response of modules 37m and 47m (transmit, 1326 MHz, averaged over ten pulse trains)

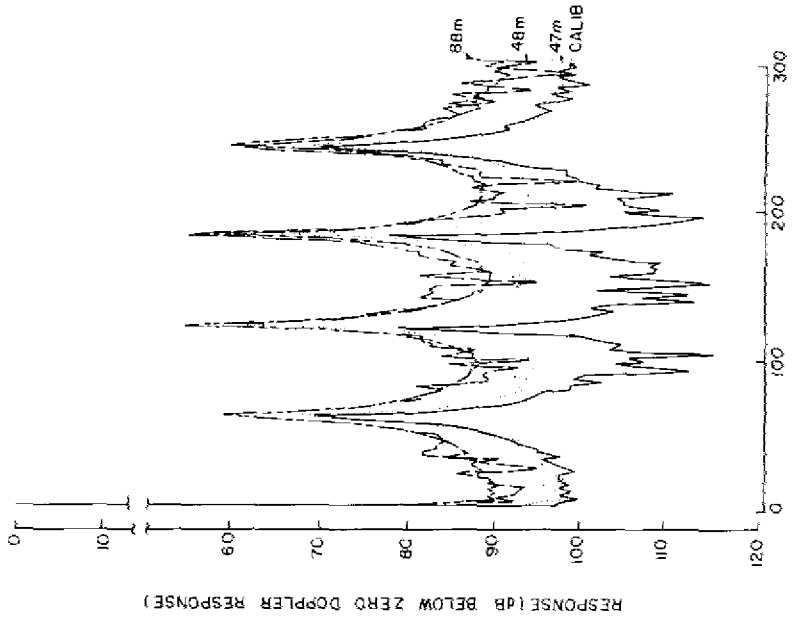

Fig. 17 — Spectral response (nulled response or C_1 data) of modules 47m, 48m, and 88m (transmit, 1266 MHz, averaged over ten pulse trains)

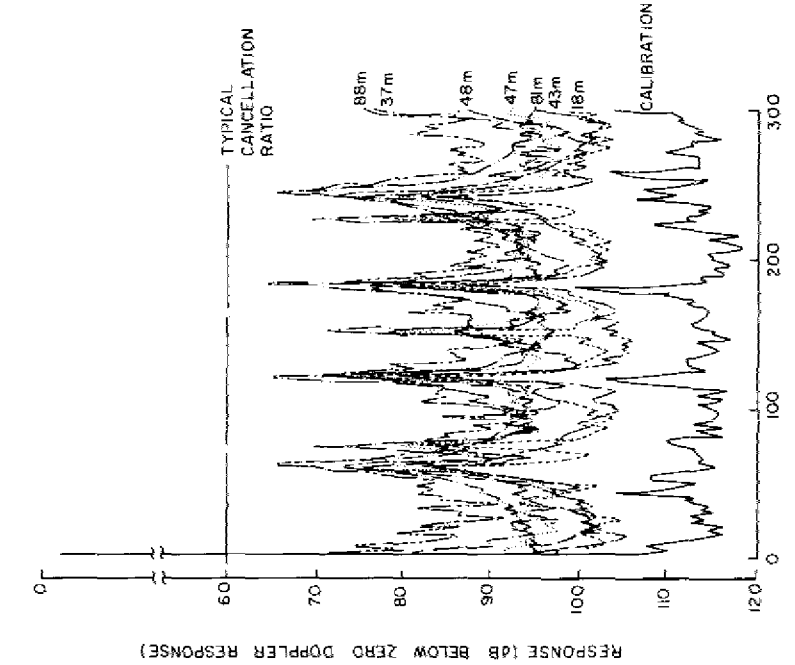

Fig. 16 — Spectral response (nulled response, or C_1 data) of modules 18m, 37m, 43m, 47m, 48m, 81m, and 88m (transmit, 1326 MHz, averaged over ten pulse trains)

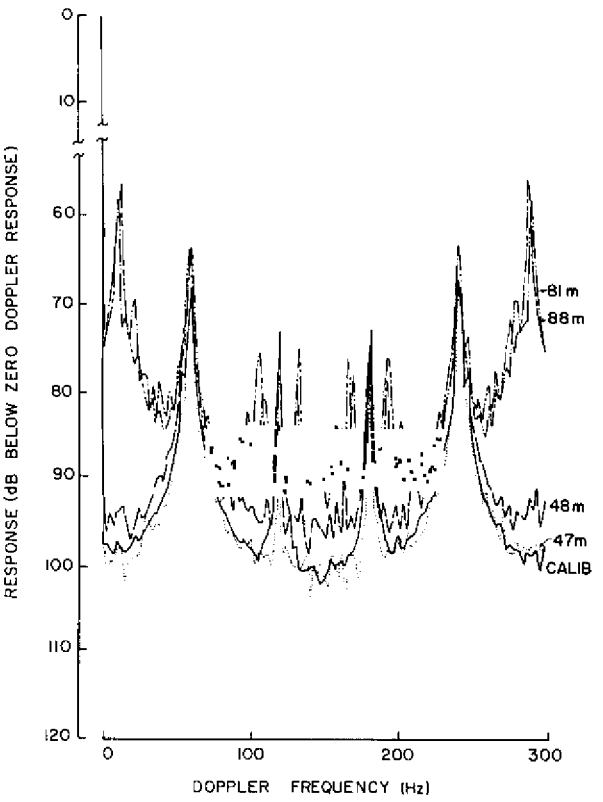

Fig. 18 — Spectral response (nulled response, or C_1 data) of modules 47m, 48m, 81m, and 88m (transmit, 1383 MHz, averaged over ten pulse trains)

Figure 18 shows the spectra of modules 47m, 48m, 81m, and 88m in the transmit mode at 1383 MHz.

Figures 19, 20, and 21 show the spectra of modules 48m and 81m in the receive mode at the low, mid, and high frequencies respectively. These plots indicate that the spectra introduced by the modules in the receive mode are substantially below that introduced in the transmit mode. This is as expected, since the receiver sections of the module use low-power low-stress-level class-A devices, whereas the transmit sections employ high-power high-stress-level class-B and class-C devices.

Figures 22, 23, and 24 are plots of spectra obtained when modules are connected in a cascaded fashion. Two pairs of modules were connected in cascade and observed at the low, mid, and high frequencies respectively. The cascaded configuration consisted of one module in the transmit mode feeding (through appropriate attenuation) the second module in the receive mode. The module listed first was in the transmit mode. These plots therefore show the combined effect of the two modules under conditions which are quite similar to an AEW system using these solid-state modules for both the transmit and receive functions.

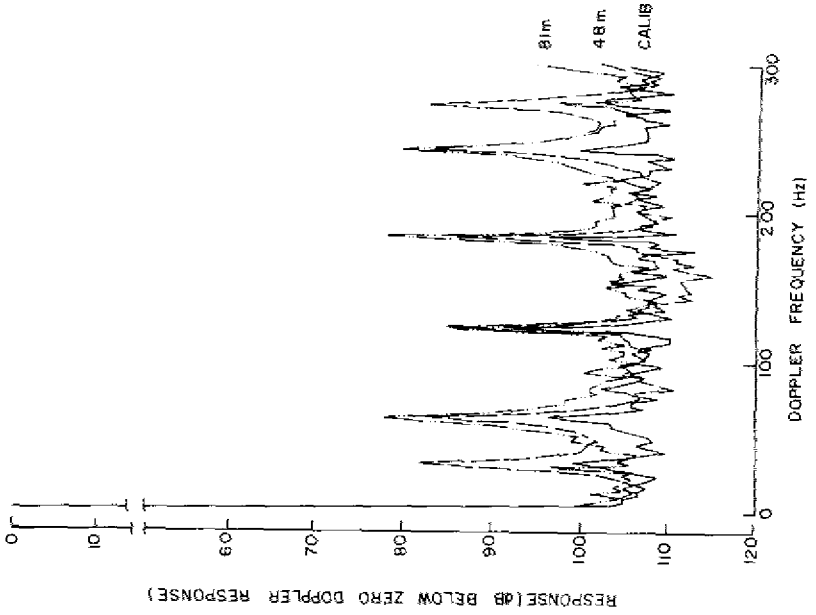

Fig. 20 — Spectral response (nulled response, or C_1 data) of modules 48m and 81m (receive, 1326 MHz, averaged over ten pulse trains)

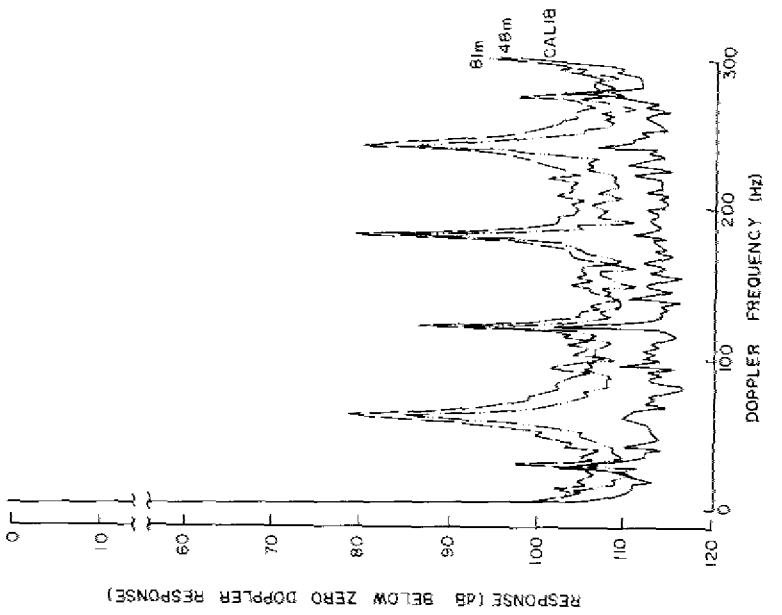

Fig. 19 — Spectral response (nulled response, or C_1 data) of modules 48m and 81m (receive, 1266 MHz, averaged over ten pulse trains)

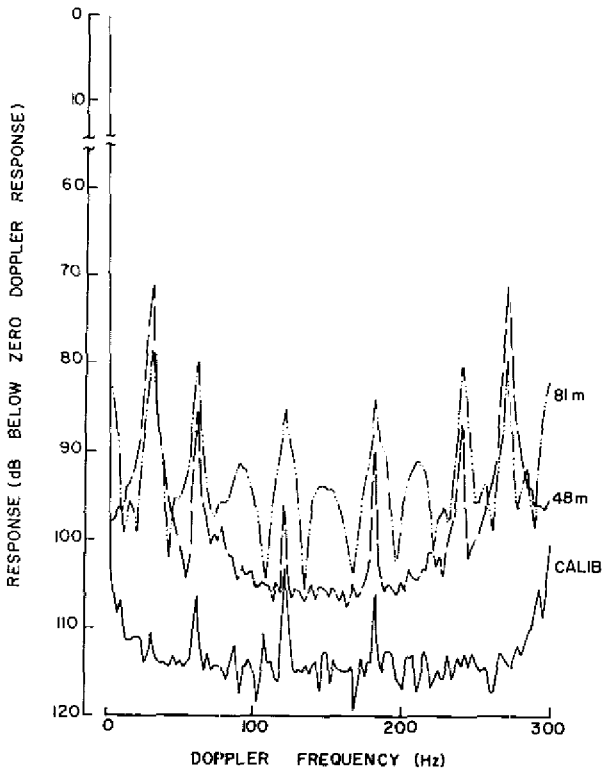

Fig. 21 — Spectral response (nulled response, or C_1 data) of modules 48m and 81m (receive, 1333 MHz, averaged over ten pulse trains)

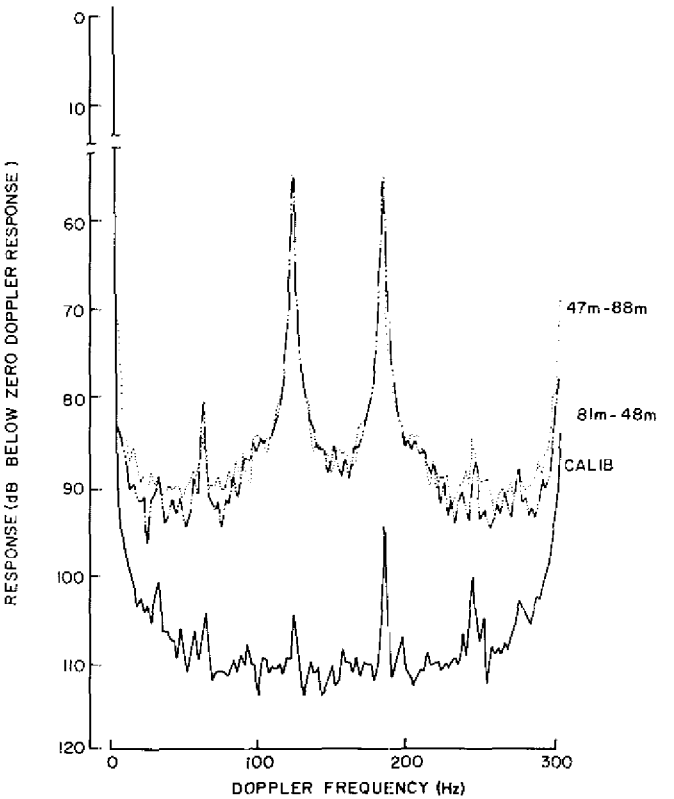

Fig. 22 — Spectral response (nulled response, or C_1 data) of modules 47m and 88m in a cascaded configuration (first module in the transmit mode and the second module in the receive mode) and modules 81m and 48m in a cascaded configuration (1266 MHz, averaged over ten pulse trains)

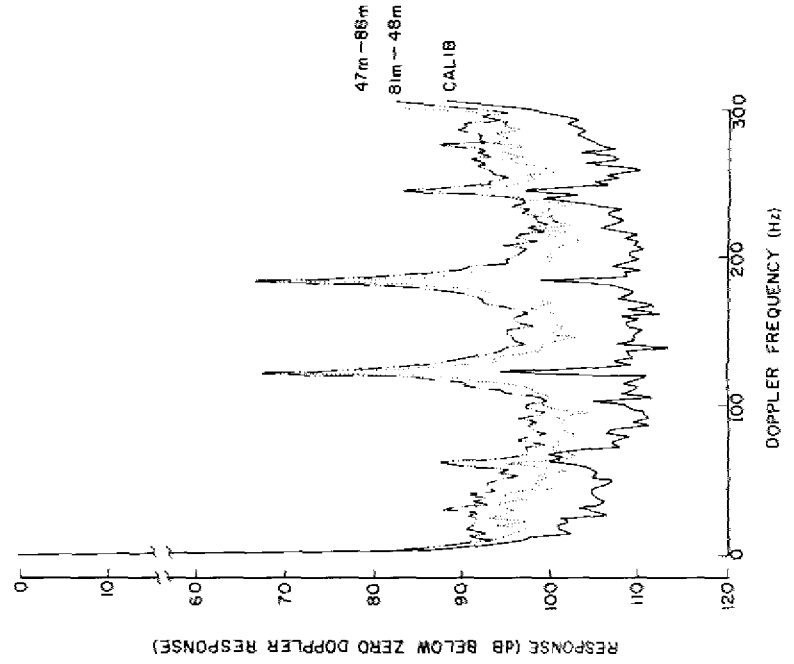

Fig. 24 — Spectral response (nulled response, or C_1 data) of modules 47m and 88m in a cascaded configuration and modules 81m and 48m in a cascaded configuration (1383 MHz, averaged over ten pulse trains)

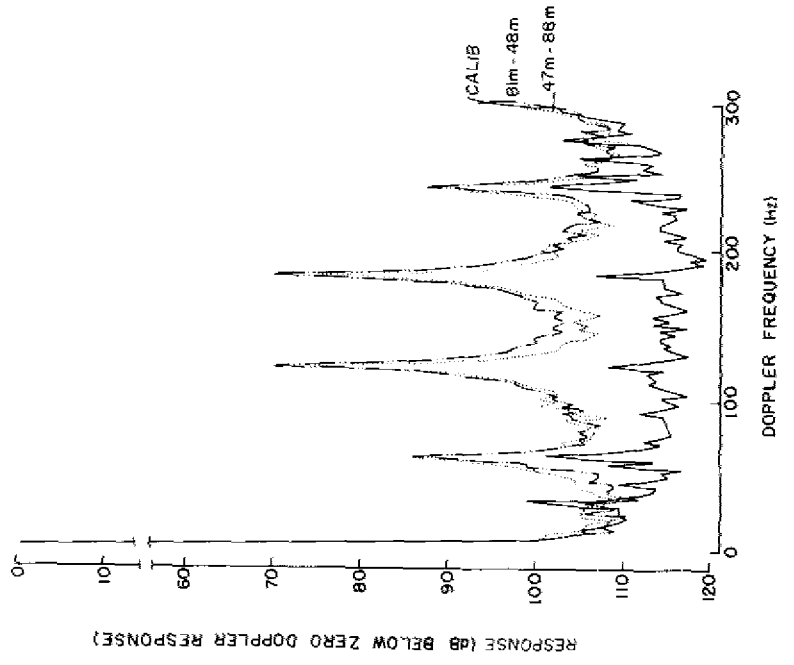

Fig. 23 — Spectral response (nulled response, or C_1 data) of modules 47m and 88m in a cascaded configuration and modules 81m and 48m in a cascaded configuration (1326 MHz, averaged over ten pulse trains)

These measurements provide a sensitive indication of module performance. This becomes apparent when the frequency of the peaks is considered.

There are additional peaks which do not correlate with the power-supply ripple or its harmonics. For instance, Fig. 13 shows peaks at doppler frequencies of approximately 60, 80, 120, 150, 180, 220, and 240 Hz. The peaks at 60, 120, 180, and 240 Hz correlate with the power-supply ripple or its harmonics and will be ignored here. The peaks at 80, 150, and 220 Hz do not correlate with the power-supply ripple and are attributed to the modules. These peaks would be present in a target-free environment. They will tend to mask targets at these doppler frequencies. The plot shows the level of these peaks relative to the normal signal or zero-doppler response. The peaks at 80, 150, and 220 Hz are 76, 73, and 73 dB down from the zero doppler response, and this would represent the limitation on the detection capability in an AEW system.

No attempt will be made at this time to account for the remaining peaks or sidebands except to note that they do appear to be contributed by the module. They were observed consistently for a number of different modules in various test conditions. Further, they were not present in any of the calibration runs, when a suitable length of cable was substituted for the module.

The presence of these peaks tends to establish a limit on the detection capability of an AEW system using these modules at these doppler frequencies. The distortion that is represented by the peaks will not be canceled by any known "comparison" or cancellation technique. The signal-to-distortion ratio is in effect a limitation to the attainable improvement factor. At the doppler frequency where the distortion appears, the upper limit on the improvement factor is the signal-to-distortion ratio. Or, stated in a slightly different manner, the detection capability of the radar at the doppler frequency of the distortion is limited by the signal-to-distortion ratio.

The impact of the pulse-to-pulse variations indicated by these spectra on present-day AEW systems will be minimal, since the typical improvement factor is below this level. A typical improvement factor is 60 dB. Thus a comfortable margin of some 13 to 16 dB exists between the level of the observed spectra and present detection capability.

ACKNOWLEDGMENTS

The author acknowledges the contributions of Drs. G. A. Andrews, T. L. ap Rhys, and W. K. Kahn during all phases of this effort. The author also acknowledges the contribution of Mr. Arlie Long of NRL and Dr. David Staiman of RCA, Moorestown, for assisting in the design of the experimental apparatus and performing the measurements.

REFERENCES

1. C.E. Cook and M. Bernfeld, "Radar Signals, An Introduction to Theory and Application," Academic Press, New York, London, Ch. 11, 1967.

2. S. Goldman, *Frequency Analysis, Modulation, and Noise*, McGraw-Hill, New York, 1948.

3. D. Staiman and J. Liston, "Fidelity of Pulsed Microwave Transistor Amplifiers," *Proceedings of the IEE S-MTT International Microwave Symposium*, pp. 130-131, June 1974.

4. D. Staiman, "L-Band Transceiver Module Fidelity Test Program," contract N00173-75-C-0507 Data Item A0002, Final report, Sept. 1975.

5. J.S. Bendat and A.G. Pierson, "Measurement and Analysis of Random Data," J. Wiley, New York, Ch. 7, 1966.

6. H.A. Wheeler, "The Interpretation of Amplitude and Phase Distortion in Terms of Paired Echoes," *Proc. I.R.E.* 27, 359-385 (June 1939).

7. A. Papoulis, *Systems and Transforms with Applications in Optics*, McGraw-Hill, New York, 1968.